Journal of Low Temperature Physics
https://doi.org/10.1007/s10909-024-03068-3

# Current-Dependent Resistance in TES Wiring Superimposed *Nb* Striplines

**Lorenzo Ferrari Barusso[1,2] · Edvige Celasco[1,2] · Giovanni Gallucci[2] · Daniele Grosso[1,2] · Luca Repetto[1] · Manuela Rigano[1,2] · Matteo D'Andrea[3] · Claudio Macculi[3] · Guido Torrioli[4] · Flavio Gatti[1,2]**

Received: 3 November 2023 / Accepted: 26 February 2024


## Abstract
During the characterization of the demonstration model of the Cryogenic AntiCoincidence (CryoAC) Detector (ACS-10), a current-dependent parasitic resistance was found in series with the TES network on board the detector. Analysis was possible because the resistance rises for currents above 11 $\mu$A, and is therefore not observed at low bias excitation. A comparison of measurements of the TES across its *Nb* wiring at different temperatures suggested that the source of resistance was in the wiring and not in the TES network. After several analysis of the wiring fabrication steps, FIB-FE-SEM studies of film sections and tests of niobium film quality, we understood that the parasitic resistance was due to point contact in the *Nb* step coverage caused by film cracks. The fracture was due to the wall steepness and thickness of the films, since rapid step coverage is less mechanically stable and the stress on the films is proportional to the fourth power of the thickness. Therefore, all thicknesses in the wiring were reduced to the minimum optimum step coverage values and the first negative lithography parameters were optimized to reduce the wall film angle. The samples after this optimization showed no current-dependent series resistance to TES.

**Keywords** Wiring · Niobium film · Stripline · Parasitic resistance · TES

✉ Lorenzo Ferrari Barusso
lorenzo.ferrari@ge.infn.it

Matteo D'Andrea
matteo.dandrea@inaf.it

1 Physics Department, Università di Genova, Via Dodecaneso 33, 16146 Genova, Italy

2 Sezione di Genova, INFN, via Dodecaneso 33, 16146 Genova, Italy

3 IAPS, INAF, Via del Fosso del Cavaliere, 100, 00133 Roma, Italy

4 IFN, CNR, Via del Fosso del Cavaliere, 100, 00133 Roma, Italy

Published online: 18 March 2024

## 1 Introduction

During the development of the Cryogenic AntiCoincidence (CryoAC) detector [1] for the Athena X-IFU [2], we developed a fully functional detector (ACS-10) [3] to demonstrate the operation of the CryoAC. For this purpose, the detector was integrated at SRON to work together with the NASA TES array [4] with good results [5], demonstrating the anticoincidence capabilities. However, the characterization of ACS-10 [6] revealed a current-dependent parasitic resistance $R_P$ in series with the TES network. See Fig. 1. Therefore, the behaviour of the detector was investigated to understand the nature of the parasitic resistance and then solved to produce new detectors without the issue. The parasitic resistance increases the power dissipated at cold and reduces the performance of the detector. Key aspects in the reformulation of the mission towards the development of the CryoAC for the NewAthena X-IFU.

## 2 Investigations and Resolution

Looking at the ACS-10 IV curves at different temperatures [6] was clear that the resistance was on the absorber of the detector as changing the temperature of the cryostat or using the heaters on board the detector produced the same IV characteristics. Then the possible sources for the parasitic resistance could have been inside the *Ir*/*Au* TES film properties or in the *Nb* striplines. Taking section images of the *Nb* wiring using focused ion beam (FIB) etchings and field-effect SEM (FE-SEM) microscope, we were able to spot breakages in the upper *Nb* stripline corresponding to step coverage. See Fig. 2 (left). Our wiring is made by two *Nb* striplines one above the other separated with a $SiO_x$ layer. Structures are obtained through lift-off, depositing one layer after the previous structure is concluded [3].

The point contact inside niobium led to a resistance in series to the TES network that is superconductive for currents lower than 11 $\mu A$. The $J_c$ calculated

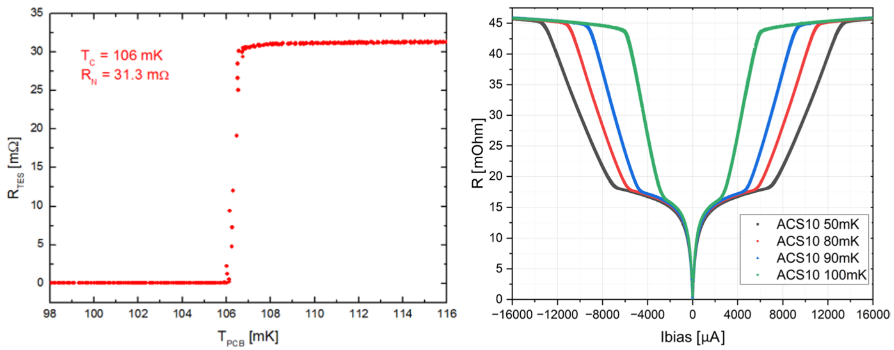


**Fig. 1** Left) Transition curve of the ACS-10 TES array. Measurement have been taken with a 1 $\mu$A bias current and in 4-probe configuration. - Right) TES circuit resistance versus bias current. It is clear as with a small current in the circuit ~ 11 $\mu A$ a parasitic resistance of ~ 15 mΩ rises since the transition of TESs that have then a 46 mOhm apparent resistance

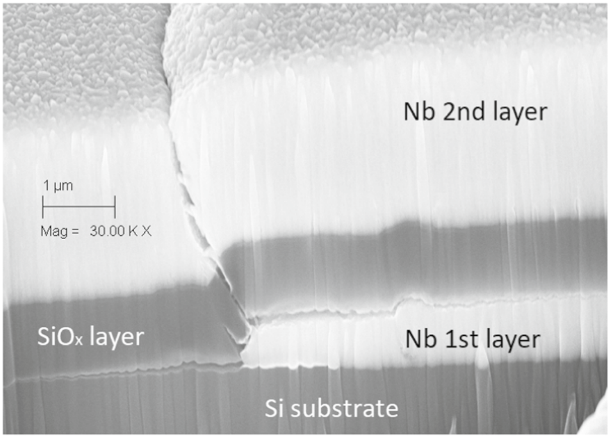


**Fig. 2** Section FE-SEM image acquired through a FIB etching of *Nb* step coverage in a ACS-10 same batch detector wiring. A breakage in $SiO_x$ and upper *Nb* is clearly visible, leading to point contact and low critical current in *Nb* wiring

respect to the wiring geometry was of 0.7 $\frac{\text{A}}{\text{cm}^2}$, while at 100 mK the $J_c$ of ACS-10 TES is 4.2 $\frac{A}{cm^2}$ and the one of our niobium films is higher than $3.9 \times 10^5$ $\frac{\text{A}}{\text{cm}^2}$ at 4.2 K.

Due to this issue, we explored the possibility of a parallel *Nb* wiring detector with less TES [7, 8]. However, after several analysis of the wiring production steps, investigations and tests we understood that the film breakage was due to the film wall steepness and thickness as a rapid step coverage is less mechanically stable. We tested the mechanical properties of our *Nb* films' varying thickness and deposition parameters. Thermal cycles of those samples did not reveal any substantial stress in the film itself. Thus, we concentrated on reducing the wall film angle to promote subsequent film grows [9]. The first negative lithography parameters have been tuned, finding an optimal value in a 3 $\mu$m under-etching on the resist film, with over-develop process, to deposit *Nb* under the resist. At this point, to promote the isotropy of *Nb* deposition parameters have been tuned reducing *Ar* sputtering pressure and increasing RF power. However, this did not solved completely the issue as some voids in the oxide layer and in the upper *Nb* strip were still present. Then, we studied the relations between each film layer finding a criticity in thermal relaxations of the $SiO_x$ film respect to the *Nb* ones and in the oxide layer rigidity. In the end, all wiring layer thicknesses were reduced to the minimum optimal step coverage values with each layer 1.5 times thicker than the underneath one to minimize the thermal relaxation mismatch and the $SiO_x$ rigidity [9, 10]. In Fig. 3 (right) is shown the new wiring profile without breakage in films.

Thereafter, several samples have been produced and measured. In Fig. 4, a comparison between the TES current and tension of ACS-10 with one of the DM#70 produced with the new wiring procedure is presented. These measurements as well

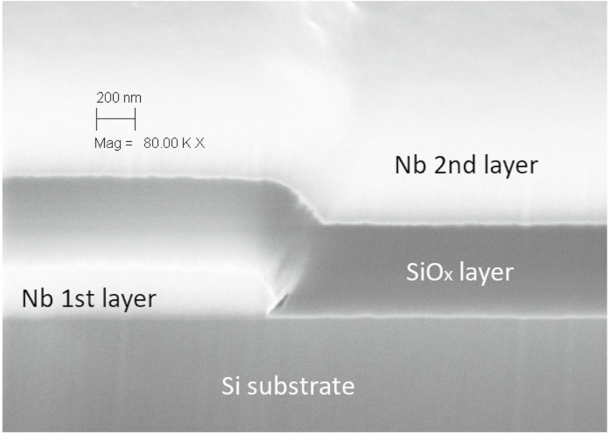


**Fig. 3** Section FE-SEM image acquired through a FIB etching of *Nb* step coverage in new wiring fabrication procedure batch. Films are smoother and the step coverage is done without any breakage

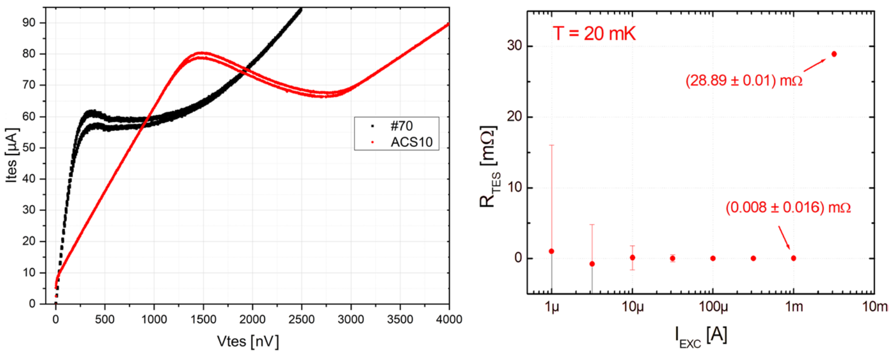


**Fig. 4** Left) IV comparison between ACS-10 and sample #70 produced with the new wiring procedure. In the sample #70 is evident the absence of the slope before the TES transition corresponding to the parasitic resistance. - Right) Resistance versus bias current in the sample #70. Until the bias current reaches the TES array critical current value ~ 1 mA, the values measured are compatible with 0

all the tests carried out with new wiring procedure samples highlighted the absence of the current-dependent parasitic resistance.

## 3 Conclusion

The current-dependent parasitic resistance that affected the Demonstration Model of the CryoAC ACS-10 was found to reside in the *Nb* wirings. A complete understanding of the generation phenomena was possible leading to the production of detectors without issue and with resistances in superconducting state < 30 mΩ up

**Table 1** Resistance values in TES circuit due to TES normal resistance, old and new *Nb* wirings

| Contributions to TES circuit | Typical values with old wiring | Typical values with new wiring |
|---|---|---|
| TES normal state resistance | ~ 30 mΩ | ~ 30 mΩ |
| Residual resistance | < 0.03 mΩ | < 0.03 mΩ |
| Current-dependent resistance | ~ 15 mΩ | < 0.03 mΩ |

to 1 m*A* bias currents. See Fig. 4 and Table 1. This is a good point in the development of the CryoAC of the NewAthena X-IFU as the parasitic resistance would have implied a higher power dissipation, while power loads are a critical point in the mission requirements.

**Acknowledgements** The authors would like to thank A. Bevilacqua, F. Siccardi and L. Parodi for their technical support.

**Funding** Open access funding provided by Università degli Studi di Genova within the CRUI-CARE Agreement.



## References

1. C. Macculi, A. Argan, D. Brienza, M. D'Andrea, S. Lotti, G. Minervini, L. Piro, M. Biasotti, L. Ferrari Barusso, F. Gatti, M. Rigano, G. Torrioli, M. Fiorini, S. Molendi, M. Uslenghi, E. Cavazzuti, A. Volpe, The cryogenic anticoincidence detector for ATHENA X-IFU: the project status. J. Low Temp. Phys. **199**(1–2), 416–424 (2020). https://doi.org/10.1007/s10909-019-02314-3
2. D. Barret, V. Albouys, J.-W.D. Herder, L. Piro, M. Cappi, J. Huovelin, R. Kelley, J.M. Mas-Hesse, S. Paltani, G. Rauw, A. Rozanska, J. Svoboda, J. Wilms, N. Yamasaki, M. Audard, S. Bandler, M. Barbera, X. Barcons, E. Bozzo, M.T. Ceballos, I. Charles, E. Costantini, T. Dauser, A. Decourchelle, L. Duband, J.-M. Duval, F. Fiore, F. Gatti, A. Goldwurm, R.D. Hartog, B. Jackson, P. Jonker, C. Kilbourne, S. Korpela, C. Macculi, M. Mendez, K. Mitsuda, S. Molendi, F. Pajot, E. Pointecouteau, F. Porter, G.W. Pratt, D. Prêle, L. Ravera, K. Sato, J. Schaye, K. Shinozaki, K. Skup, J. Soucek, T. Thibert, J. Vink, N. Webb, L. Chaoul, D. Raulin, A. Simionescu, J.M. Torrejon, F. Acero, G. Branduardi-Raymont, S. Ettori, A. Finoguenov, N. Grosso, J. Kaastra, P. Mazzotta, J. Miller, G. Miniutti, F. Nicastro, S. Sciortino, H. Yamaguchi, S. Beaumont, E. Cucchetti, M. D'Andrea, M. Eckart, P. Ferrando, E. Kammoun, S. Lotti, J.-M. Mesnager, L. Natalucci, P. Peille, J. Plaa, F. Ardellier, A. Argan, E. Bellouard, J. Carron, E. Cavazzuti, M. Fiorini, P. Khosropanah, S. Martin, J. Perry, F. Pinsard, A. Pradines, M. Rigano, P. Roelfsema, D. Schwander, G. Torrioli, J. Ullom, I. Vera, E.M. Villegas, M. Zuchniak, F. Brachet, U.L. Cicero, W. Doriese, M. Durkin, V. Fioretti, H. Geoffray, L. Jacques, C. Kirsch, S. Smith, J. Adams, E. Gloaguen, R. Hoogeveen, P. Hulst, M. Kiviranta, J. Kuur, A. Ledot, B.-J. Leeuwen, D. Loon, B. Lyautey, Y. Parot, K. Sakai, H. Weers, S. Abdoelkariem, T. Adam, C. Adami, C. Aicardi, H. Akamatsu, P.E.M. Alonso, R. Amato, J. André, M. Angelinelli, M. Anon-Cancela, S. Anvar, R. Atienza, A. Attard, N. Auricchio, A. Balado, F. Bancel, L.F. Barusso,

A. Bascuñan, V. Bernard, A. Berrocal, S. Blin, D. Bonino, F. Bonnet, P. Bonny, P. Boorman, C. Boreux, A. Bounab, M. Boutelier, K. Boyce, D. Brienza, M. Bruijn, A. Bulgarelli, S. Calarco, P. Callanan, A.P. Campello, T. Camus, F. Canourgues, V. Capobianco, N. Cardiel, F. Castellani, O. Cheatom, J. Chervenak, F. Chiarello, L. Clerc, N. Clerc, B. Cobo, O. Coeur-Joly, A. Coleiro, S. Colonges, L. Corcione, M. Coriat, A. Coynel, F. Cuttaia, A. D'Ai, F. D'anca, M. Dadina, C. Daniel, L. Dauner, N. DeNigris, J. Dercksen, M. DiPirro, E. Doumayrou, L. Dubbeldam, M. Dupieux, S. Dupourqué, J.L. Durand, D. Eckert, V. Eiriz, E. Ercolani, C. Etcheverry, F. Finkbeiner, M. Fiocchi, H. Fossecave, P. Franssen, M. Frericks, S. Gabici, F. Gant, J.-R. Gao, F. Gastaldello, L. Genolet, S. Ghizzardi, M.A.A. Gil, E. Giovannini, O. Godet, J. Gomez-Elvira, R. Gonzalez, M. Gonzalez, L. Gottardi, D. Granat, M. Gros, N. Guignard, P. Hieltjes, A.J. Hurtado, K. Irwin, C. Jacquey, A. Janiuk, J. Jaubert, M. Jiménez, A. Jolly, T. Jourdan, S. Julien, B. Kedziora, A. Korb, I. Kreykenbohm, O. König, M. Langer, P. Laudet, P. Laurent, M. Laurenza, J. Lesrel, S. Ligori, M. Lorenz, A. Luminari, B. Maffei, O. Maisonnave, L. Marelli, D. Massonet, I. Maussang, A.G. Melchor, I. Le Mer, F.J.S. Millan, J.-P. Millerioux, T. Mineo, G. Minervini, A. Molin, D. Monestes, N. Montinaro, B. Mot, D. Murat, K. Nagayoshi, Y. Nazé, L. Noguès, D. Pailot, F. Panessa, L. Parodi, P. Petit, E. Piconcelli, C. Pinto, J.M.E. Plaza, B. Plaza, D. Poyatos, T. Prouvé, A. Ptak, S. Puccetti, E. Puccio, P. Ramon, M. Reina, G. Rioland, L. Rodriguez, A. Roig, B. Rollet, M. Roncarelli, G. Roudil, T. Rudnicki, J. Sanisidro, L. Sciortino, V. Silva, M. Sordet, J. Soto-Aguilar, P. Spizzi, C. Surace, M.F. Sánchez, E. Taralli, G. Terrasa, R. Terrier, M. Todaro, P. Ubertini, M. Uslenghi, J.G.B. Vaate, D. Vaccaro, S. Varisco, P. Varnière, L. Vibert, M. Vidriales, F. Villa, B.M. Vodopivec, A. Volpe, C. Vries, N. Wakeham, G. Walmsley, M. Wise, M. Wit, G. Woźniak, The ATHENA x-ray integral field unit: a consolidated design for the system requirement review of the preliminary definition phase. Exp. Astron. **55**(2), 373–426 (2023). https://doi.org/10.1007/s10686-022-09880-7

3. M. Biasotti, C. Boragno, L. Ferrari Barusso, F. Gatti, D. Grosso, M. Rigano, B. Siri, C. Macculi, M. D'Andrea, L. Piro, The phonon-mediated TES cosmic ray detector for focal plane of ATHENA x-ray telescope. J. Low Temp. Phys. **199**(1–2), 225–230 (2020). https://doi.org/10.1007/s10909-020-02348-y
4. S.J. Smith, J.S. Adams, S.R. Bandler, S. Beaumont, J.A. Chervenak, E.V. Denison, W.B. Doriese, M. Durkin, F.M. Finkbeiner, J.W. Fowler, G.C. Hilton, R. Hummatov, K.D. Irwin, R.L. Kelley, C.A. Kilbourne, M.A. Leutenegger, A.R. Miniussi, F.S. Porter, C.D. Reintsema, J.E. Sadleir, K. Sakai, D.S. Swetz, J.N. Ullom, L.R. Vale, N.A. Wakeham, E.J. Wassell, M.C. Witthoeft, Performance of a broad-band, high-resolution, transition-edge sensor spectrometer for x-ray astrophysics. IEEE Trans. Appl. Supercond. **31**(5), 1–6 (2021). https://doi.org/10.1109/tasc.2021.3061918
5. M. D'Andrea, K. Ravensberg, A. Argan, D. Brienza, S. Lotti, C. Macculi, G. Minervini, L. Piro, G. Torrioli, F. Chiarello, L. Ferrari Barusso, M. Biasotti, G. Gallucci, F. Gatti, M. Rigano, H. Akamatsu, J. Dercksen, L. Gottardi, F. Groote, R. Hartog, J.-W. Herder, R. Hoogeveen, B. Jackson, A. McCalden, S. Rosman, E. Taralli, D. Vaccaro, M. Wit, J. Chervenak, S. Smith, N. Wakeham, Athena X-IFU demonstration model: first joint operation of the main TES array and its cryogenic anticoincidence detector (CryoAC). J. Low Temp. Phys. **209**(3–4), 433–440 (2022). https://doi.org/10.1007/s10909-022-02786-w
6. M. D'Andrea, C. Macculi, G. Torrioli, A. Argan, D. Brienza, S. Lotti, G. Minervini, L. Piro, M. Biasotti, L. Ferrari Barusso, F. Gatti, M. Rigano, A. Volpe, E.S. Battistelli, The demonstration model of the ATHENA X-IFU cryogenic anticoincidence detector. J. Low Temp. Phys. **199**(1–2), 65–72 (2019). https://doi.org/10.1007/s10909-019-02300-9
7. C. Macculi, A. Argan, M. D'Andrea, S. Lotti, G. Minervini, L. Piro, L. Ferrari Barusso, C. Boragno, E. Celasco, G. Gallucci, F. Gatti, D. Grosso, M. Rigano, F. Chiarello, G. Torrioli, M. Fiorini, M. Uslenghi, D. Brienza, E. Cavazzuti, S. Puccetti, A. Volpe, P. Bastia, The cryogenic anticoincidence detector for the newAthena X-IFU instrument: a program overview. Condens. Matter. **8**(4), 108 (2023). https://doi.org/10.3390/condmat8040108
8. M. D'Andrea, C. Macculi, S. Lotti, L. Piro, A. Argan, G. Minervini, G. Torrioli, F. Chiarello, L. Ferrari Barusso et al., The TES-based cryogenic anticoincidence detector (CryoAC) of ATHENA X-IFU: a large area silicon microcalorimeter for background particles detection. J. Low Temp. Phys. **214**(3), 164–172 (2024). https://doi.org/10.1007/s10909-023-03034-5
9. A.G. Evans, J.W. Hutchinson, The thermomechanical integrity of thin films and multilayers. Acta Metall. Mater. **43**(7), 2507–2530 (1995). https://doi.org/10.1016/0956-7151(94)00444-m
10. P. Vretenar, Mechanical stresses in oxide thin films. Vacuum **43**(5–7), 727–729 (1992). https://doi.org/10.1016/0042-207x(92)90119-h